Journal of Solid State Chemistry **156,** 305–312 (2001)
doi:10.1006/jssc.2000.8999, available online at http://www.idealibrary.com on IDEAL®

A Mixed α/β Superstructure in NASICON Ionic Conductors: Neutron Diffraction Study of $Li_2FeTi(PO_4)_3$ and $Li_2FeZr(PO_4)_3$

Michele Catti

Dipartimento di Scienza dei Materiali, Università di Milano Bicocca, via Cozzi 53, 20125 Milano, Italy
E-mail: catti@mater.unimib.it

Received June 20, 2000; in revised form September 11, 2000; accepted October 6, 2000; published online January 3, 2001

The lithium conductors $Li_2FeTi(PO_4)_3$ and $Li_2FeZr(PO_4)_3$, synthesized by solid-state reaction and characterized by X-ray powder diffractometry, were studied structurally at room temperature by neutron powder diffraction at high resolution (HRPD, ISIS Facility, U.K.). By trial-and-error and Rietveld refinements ($R_p = 0.111$, $R(F^2) = 0.112$), the first compound (orthorhombic *Pbca*, $Z = 8$; $a = 8.5515(1)$, $b = 8.6229(1)$, $c = 23.9116(3)$ Å) was shown to have a complex superstructure sharing features of both the α and β NASICON-type phases of $LiZr_2(PO_4)_3$. Four (001) layers of PO_4 and (Fe, Ti)O_6 polyhedra are present per unit-cell, and they are related both by $\bar{1}$ inversion centers (α structure) and by *a* glide planes (β structure). Ti^{4+} and Fe^{3+} order in the two interlayer regions, respectively. Owing to the structure complexity, only half of the lithium atoms could be refined in tetrahedral coordination with $\langle$Li–O$\rangle = 1.99$ Å. $Li_2FeZr(PO_4)_3$ (orthorhombic *Pbna*, $Z = 4$; $a = 8.70559(8)$, $b = 8.78572(9)$, $c = 12.2202(1)$ Å) proved to be similar to β-$LiZr_2(PO_4)_3$; however, by Fourier synthesis and Rietveld refinement ($R_p = 0.0618$, $R(F^2) = 0.0574$) Li was located in a fully ordered tetrahedral configuration with $\langle$Li–O$\rangle = 2.01$ Å, instead of being disordered as in the β phase of $LiZr_2(PO_4)_3$. © 2001 Academic Press

Key Words: **neutron diffraction; Rietveld refinement; ionic conductivity; $Li_2FeTi(PO_4)_3$; $Li_2FeZr(PO_4)_3$.**

INTRODUCTION

In the search for new materials to be employed either as electrodes or as solid electrolytes in rechargeable lithium batteries (1), the NASICON-type system $Li_{1+x}M'M''(PO_4)_3$ has been playing a major role for several years (2–4). Improving the electrical and electrochemical performances of such materials requires a full knowledge of the atomistic mechanisms of lithium transport, and hence of the crystal structure details of the phases involved, with a special stress on the coordination environment and order–disorder state of lithium atoms.

With this aim, a research program was undertaken to elucidate the structural properties of this complex system by the technique of high-resolution neutron powder diffraction. As a first step, $LiZr_2(PO_4)_3$ was reconsidered and the structural aspects of its polymorphism were fully clarified (5–7), so as to account for the different ionic conductivities of its four modifications on an atomistic basis. In particular, all polymorphs contain slabs of Oc_2T_3 ($Oc = ZrO_6$ octahedron, $T = PO_4$ tetrahedron) units with orientations (102) and (001) in the high-temperature polymorphs α (trigonal $R\bar{3}c$) and β (orthorhombic *Pbna*[1]), respectively. The α and β structures differ simply by the way the slabs are stacked: adjacent layers are related by $\bar{1}$ inversion centeres in the former case, and by *a* glide planes in the latter; in both cases the interlayer link is provided by some O atoms shared between *Oc* and *T* units belonging to neighboring slabs. Lithium ions are located in a disordered manner at the interface between slabs.

The low-temperature polymorphs α′ (triclinic $C\bar{1}$) and β′ (monoclinic $P2_1/n$)[1] are ferroelastic distortions of the previous structures, where the symmetry lowering entails an ordering process of lithium ions, which explains the smaller ionic conductivity with respect to α and β phases.

In materials with general composition $Li_{1+x}M'M''(PO_4)_3$, where M' and M'' are transition or nontransition metals with average oxidation state lower than +4, the number of lithium atoms per unit-cell increases, so that more structural sites are expected to become available for Li occupation, with a possible increase of disorder and thus of lithium mobility. Systems of this kind are $Li_3Fe_2(PO_4)_3$ and $Li_3Sc_2(PO_4)_3$ (8, 9), and $Li_{2.72}Ti_2(PO_4)_3$ (10), with β′- and β-type structures, respectively; all of them have extra occupied Li positions. A more complex system is $Li_{1+x}In_xTi_{2-x}(PO_4)_3$ (11–13): the α-type and β′-type structures were found to be stable for $x < 0.5$ and $x > 1$, respectively, while in the intermediate range $0.5 \le x \le 1.0$ a larger unit-cell with double volume and the space group *Pbca* were

[1] *Pbna*, $C\bar{1}$, $P2_1/n$: nonstandard settings of space groups *Pbcn* (no. 60), $P\bar{1}$ (no. 2), and $P2_1/c$ (no. 14).

0022-4596/01 $35.00

proposed. No account of the latter structure, however, was reported to our knowledge. Recently, the compounds $Li_2M'M''(PO_4)_3$ with M', $M'' =$ Fe, Ti, Zr were presented (14), showing that some of them would present a *Pbca* unit-cell similar to that referred to above. Some preliminary electrical conductivity measurements on these componds have also been reported (15).

In the frame of our research on lithium conductors, a structural study of $Li_2FeTi(PO_4)_3$ and $Li_2FeZr(PO_4)_3$ by high-resolution neutron powder diffraction has been carried out, with the aim of determining the crystal structure of the phase with *Pbca* symmetry and locating the extra-lithium atoms with respect to the usual NASICON-type phases. Results of conductivity measurements by complex impedence spectroscopy on these materials are reported elsewhere (16).

EXPERIMENTAL

$Li_2FeTi(PO_4)_3$ (F.W. = 402.543) and $Li_2FeZr(PO_4)_3$ (F.W. = 445.863) were synthesized by solid-state reaction (14), starting from reagent grade Li_2CO_3, $NH_4H_2PO_4$, Fe_2O_3, and TiO_2 or ZrO_2 mixed in stoichiometric ratios. The samples were put in a Pt boat and heated for 4 h at 600°C in a tubular furnace; then they were ground and pelletized and heated for 8 h at 1090°C. Powder X-ray diffractometry (Bruker D8 Advance apparatus with θ–θ geometry, Cu$K\alpha$ radiation, graphite monochromator on the diffracted beam) was used to characterize the compounds obtained, with the following experimental conditions: fixed divergence (0.5°), scattering (0.5°), and detector (0.03°) slits, counting time 10 s/step, step width $\Delta(2\theta) = 0.02°$. The $Li_2FeZr(PO_4)_3$ sample proved to be pure β-type orthorhombic *Pbna* phase, with the following unit-cell constants: $a = 8.693(2)$, $b = 8.774(2)$, $c = 12.208(2)$ Å. $Li_2FeTi(PO_4)_3$ turned out also to be single-phase, and its X-ray powder pattern (Fig. 1) was indexed by identifying superlattice Bragg peaks corresponding to a doubled c cell edge, in addition to peaks analogous to those observed in the previous compound. The unit-cell parameters were least-squares refined on the basis of the 2θ values of 25 peaks, using a homemade computer routine, and obtaining the following values: $a = 8.557(3)$, $b = 8.624(3)$, $c = 23.919(6)$ Å. Systematic absences were consistent with space group *Pbca*; the list of observed and calculated d_{hkl} values, and of the relative Bragg intensities, is given in Table 1.

Neutron diffraction data were collected on the time-of-flight High Resolution Powder Diffractometer (HRPD), equipped with a furnace, at the ISIS spallation pulsed source, Rutherford Appleton Laboratory (Chilton, U.K.). For each of the two compounds, a 2 cm^3 sample was put in a vanadium can under vacuum. By use of the backscattering counter bank at $2\theta = 168.3°$, full intensity profiles were recorded in the d_{hkl} range 0.7 to 2.5 Å (instrumental resolution $\Delta d/d \approx 4 \times 10^{-4}$) at room temperature. A preliminary data reduction was performed, including merging of outputs from single counters in the bank and correction for detector efficiency as a function of neutron wavelength.

STRUCTURE SOLUTION AND REFINEMENT

All computations, including the Rietveld refinements, were performed by the GSAS computer package (17). Chebyshev polynomials of first kind with 12 coefficients were used to model the intensity background, and the peak shape was represented by the convolution of a pseudo-Voigt

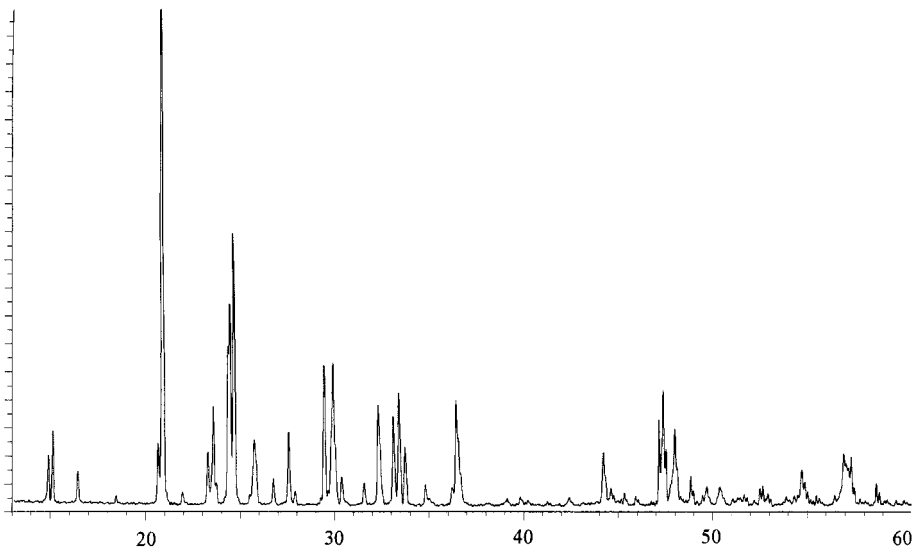

FIG. 1. X-ray powder diffraction pattern (Cu$K\alpha$ radiation) of $Li_2FeTi(PO_4)_3$. Intensity (arbitrary units) vs 2θ angle (°) is plotted.

TABLE 1
Powder Diffraction Pattern of $Li_2FeTi(PO_4)_3$ in the Range $1.5 < d_{hkl} < 6.0$ Å

h	k	l	$d_{hkl,o}$ (Å)	$d_{hkl,c}$ (Å)	I/I_{max} (%)	h	k	l	$d_{hkl,o}$ (Å)	$d_{hkl,c}$ (Å)	I/I_{max} (%)
0	0	4	5.980	5.980	6	2	2	3	2.837	2.838	4
1	1	1	5.889	5.887	10	3	0	2	2.773	2.774	18
1	1	2	5.422	5.416	4	2	1	6	2.760	2.763	4
1	1	3	4.829	4.832	2	1	3	1	2.707	2.708	15
0	2	0	4.315	4.312	7	2	2	4		2.708	
1	1	4	4.261	4.261	100	1	1	8	2.684	2.683	19
2	0	0		4.279		1	3	2	2.659	2.657	11
0	2	2	4.065	4.056	3	1	3	3	2.578	2.579	4
2	1	0	3.834	3.833	8	1	3	4	2.481	2.480	3
2	1	1	3.785	3.784	14	3	1	4	2.466	2.467	20
1	1	5	3.759	3.758	3	0	2	8	2.456	2.457	5
1	2	2	3.667	3.665	20	2	3	6	2.047	2.047	10
2	1	2	3.649	3.650	25	1	4	4	1.974	1.974	5
1	0	6	3.620	3.614	43	2	4	0	1.925	1.925	15
2	0	4	3.480	3.480	5	3	3	4	1.917	1.918	21
1	2	3	3.467	3.468	8	1	3	9	1.902	1.903	3
2	1	3	3.452	3.454	4	1	1	12	1.894	1.894	12
1	1	6	3.338	3.333	4	4	2	3	1.863	1.863	5
1	2	4	3.240	3.238	11	3	0	10	1.833	1.833	6
0	2	5	3.202	3.203	3	3	3	7	1.740	1.742	3
2	2	0	3.037	3.037	26	0	4	9	1.675	1.674	8
1	2	5	2.999	2.300	8	4	2	8	1.615	1.613	8
0	0	8	2.988	2.990	23	2	3	11	1.608	1.607	3
1	1	7	2.975	2.978	8	3	1	12	1.605	1.605	6
2	2	2	2.945	2.944	5	4	4	0	1.518	1.519	4

function (linear combination of Gaussian and Lorentzian components, with σ and γ half-widths, respectively), accounting for the sample contribution, with two back-to-back exponentials, accounting for the instrumental and moderator contributions (18). Linear dependencies of the σ and γ parameters on d_{hkl} were assumed: $\sigma = \sigma_1 d_{hkl}$, $\gamma = \gamma_1 d_{hkl}$, with σ_1 and γ_1 as refinable parameters. The mixing coefficient and the full width of the pseudo-Voigt function depend on σ and γ according to equations given in Ref. (19). A total of 14 profile parameters were included in the refinement.

$Li_2FeTi(PO_4)_3$

For solving the structure of $Li_2FeTi(PO_4)_3$, the central idea used was the layer arrangement of all NASICON-related α, β, α', and β' phases, where two layers per unit-cell are present. Such layers are related either by $\bar{1}$ centeres (α and α') or by a glide planes (β and β'). As in the present case the unit-cell corresponds to that of the β structure, but with the c edge doubled, it was assumed that four slabs were present, related by two independent symmetry operations. It was quickly found that the $a\bar{1}a\bar{1}$ stacking gave the highest overall symmetry, i.e., space group *Pbca*, while the $aa\bar{1}\bar{1}$ sequence corresponded to the monoclinic symmetry $P112/a$. Actually, other possibilities could be considered, corresponding to combinations of a and b glide planes, e.g., *aabb*, or *abab*; all of them give rise to monoclinic space groups, of type $P2/b11$ or $P112/a$. A number of these alternative structure models were tested and Rietveld refined for comparison with the orthorhombic (*Pbca*) one. However, although in some cases the R_p agreement indexes were only slightly worse, in all cases the obtained P–O and M–O interatomic distances were quite unsatisfactory, so that such structural models could be surely discarded, and the *Pbca* structure was considered to be the correct one.

The starting structural model of the *Pbca* structure was built up on the assumption of an $a\bar{1}a\bar{1}$ sequence of (001) layers, which, on the other hand, present the *aa* stacking in the β-type *Pbna* structure. Thus, the asymmetric unit (excluding Li atoms) was obtained from that of β-$LiZr_2(PO_4)_3$ (7) by applying the (pseudo)symmetry operation $\frac{1}{2} + x$, $\frac{1}{2} - y$, $\frac{1}{2} + z$, shifting the origin by $\frac{1}{4}$, $\frac{1}{4}$, $\frac{1}{4}$, and halving the ensuing z coordinates. The internal slab symmetry is lowered from $2/b$ to b; the origin is shifted from the lost inner inversion center to the acquired interlayer one, so that the new *Pbca* space group retains centrosymmetry. The generated asymmetric unit has a doubled number of independent atoms, which are related in pairs (except for P2) by the twofold pseudo-symmetry operation x, $-y$, $\frac{1}{4} - z$.

Convergence of the Rietveld refinement, including isotropic displacement factors and the site fractional

TABLE 2
Unit-Cell Constants (with e.s.d.'s in Parentheses) and Other Rietveld Refinement Results for $Li_2FeTi(PO_4)_3$ (Space Group *Pbca*, $Z = 8$) and $Li_2FeZr(PO_4)_3$ (*Pbna*, $Z = 4$)

	$Li_2FeTi(PO_4)_3$	$Li_2FeZr(PO_4)_3$
a	8.5515(1) Å	8.70559(8) Å
b	8.6229(1)	8.78572(9)
c	23.9116(3)	12.2202(1)
V	1763.20(3) Å^3	934.66(1) Å^3
Data	6298	4299
Variables	87	56
R_p	0.1110	0.0618
wR_p	0.1349	0.0772
$R(F^2)$	0.1123	0.0574

occupancies of Fe and Ti in the two available independent positions, was attained at $R_p = 0.120$. At this stage, a difference Fourier map was computed in order to locate lithium atoms. Only one negative peak ($b(\mathrm{Li}) = -0.21 \times 10^{-12}$ cm) with satisfactory distances to neighboring atoms appeared; the corresponding Li1 atom was included in the refinement, and the final cycles converged to results reported in Tables 2 and 3. The experimental, calculated, and difference diffraction profiles are shown in Fig. 2.

TABLE 3
Site Occupation Factors, Atomic Fractional Coordinates, and Isotropic Displacement Parameters of $Li_2FeTi(PO_4)_3$

	o.f.	x	y	z	U (10^{-2} Å^2)
Li1	1	0.0187(23)	0.4667(24)	0.2106(8)	0.1(1)
Fe	0.744(9)	0.5090(11)	0.2781(9)	0.1789(3)	1.5(1)
Ti	0.256(9)	0.5090(10)	0.2781(9)	0.1789(3)	1.5(1)
Fe′	0.331(8)	0.480(3)	0.7131(29)	0.0686(10)	0.2(1)
Ti′	0.669(8)	0.480(3)	0.7131(29)	0.0686(10)	0.2(1)
P1	1	0.3576(9)	0.6442(10)	0.1972(4)	0.4(2)
P1′	1	0.3467(10)	0.3665(10)	0.0519(4)	0.4(2)
P2	1	0.7900(9)	0.4888(10)	0.1200(4)	0.1(1)
O1	1	0.4112(10)	0.7016(10)	0.1411(3)	1.2(2)
O2	1	0.4207(9)	0.4893(8)	0.2146(3)	0.1(2)
O3	1	0.6860(11)	0.3877(11)	0.1586(4)	2.4(2)
O4	1	0.1804(8)	0.6483(10)	0.2009(3)	0.6(2)
O5	1	0.4203(10)	0.7642(8)	0.2443(3)	0.2(2)
O6	1	0.8929(11)	0.5840(11)	0.1613(4)	1.7(2)
O1′	1	0.3955(9)	0.3220(8)	0.1110(3)	0.1(2)
O2′	1	0.3894(9)	0.5398(8)	0.0415(3)	0.1(2)
O3′	1	0.6856(11)	0.6067(11)	0.0907(4)	1.8(2)
O4′	1	0.1706(9)	0.3536(9)	0.0466(3)	0.8(2)
O5′	1	0.4275(10)	0.2536(7)	0.0147(3)	0.5(2)
O6′	1	0.8867(10)	0.4117(9)	0.0773(3)	1.0(2)

Note. The e.s.d.'s are reported in parentheses. Corresponding primed and unprimed atoms are related by the pseudo-symmetry operation $x, -y, \frac{1}{4} - z$ ([100] pseudo-twofold axis at $y = 0, z = \frac{1}{8}$).

$Li_2FeZr(PO_4)_3$

The crystal structure of $Li_2FeZr(PO_4)_3$ was refined straightforwardly (except for Li atoms) in space group *Pbna*, on the base of isostructurality with the β phase. At convergence, difference Fourier atoms showed the presence of the missing Li atom in an ordered position with full occupancy, which was included in the refinement. The refined occupancies of Fe and Zr in the only available site did not deviate significantly from the nominal value 0.5, so that they were kept fixed. Refinement results are reported in Table 2, and the atomic coordinates and displacement factors are in Table 4. The experimental, calculated, and difference diffraction profiles are shown in Fig. 2.

DISCUSSION

The α/β Superstructure of $Li_2FeTi(PO_4)_3$

The crystal structure of $Li_2FeZr(PO_4)_3$ (Fig. 3) is based on a superlattice of the β orthorhombic unit-cell, whose c edge is doubled. The four (001) slabs contained in the supercell are related in pairs by the a glide plane (as in the β phase) and by the $\bar{1}$ inversion center (as in the α phase), so that the overall arrangement can be defined as a superstructure of both the α and β configurations. The coexistence of both structural patterns in the same unit-cell proves that a very subtle energetic balance controls the relative stability of the α and β NASICON-type modifications. An important role is probably played, in this respect, by Li atoms which are located at the interface between slabs and thus contribute to the interlayer binding. The twofold pseudo-symmetry is not consistent with the real symmetry, in the sense that there is no supergroup of space group *Pbca* which would contain that symmetry operation. This is peculiar to the present structure, because in the α' and β' cases the pseudo-twofold axis corresponds to a real symmetry axis in the more symmetrical α and β phases.

As there are two independent (pseudo-symmetrical) sites for metal cations, compositional ordering is therein allowed. The two effective ionic radii (20) are similar (0.645 and 0.605 Å for Fe^{3+} and Ti^{4+}, respectively, in octahedral coordination, vs 1.37 Å for O^{2-} with C.N. = 3 to 4) so that a chemical differentiation of the two sites is expected more on charge unbalance than on size grounds. The results of occupancy refinement show that a strong but not complete ordering of Fe/Ti over the two sites actually occurs: site 1 (Fe,Ti) is significantly richer in iron and site 1′ (Fe′, Ti′) is richer in titanium (Table 3). Adjacent (001) slabs face each other through site 1-(Fe,Ti)O_6 or through site 1′-(Fe′, Ti′)O_6 octahedra, according to whether they are related by a glide planes or by $\bar{1}$ inversion centers (Fig. 3). The two types of octahedra are shown as pale and dark gray, respectively, in Fig. 3. As site 1 and site 1′ have average charges of +3.3 and +3.7 e, respectively, it ensues that the interlayer regions

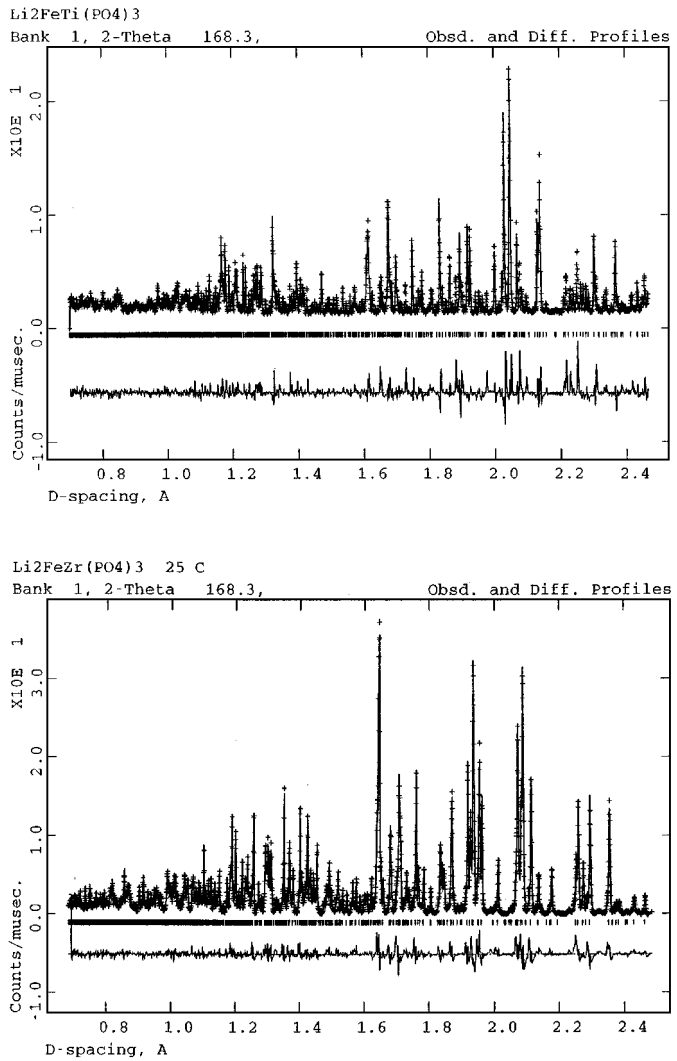

FIG. 2. Experimental (crosses), calculated, and difference profiles of the powder neutron diffraction patterns of $Li_2FeTi(PO_4)_3$ (above) and $Li_2FeZr(PO_4)_3$ (below).

across glide planes/symmetry centers are characterized by a deficit/excess of positive charge with respect to the average value $+3.5$ e. A preferential accumulation of the Li^+ ion should thus be expected in the former regions.

Indeed, the only Li atom located in the structure lies right in the neighborhood of the *a* glide plane. However, this accounts only for half of the lithium content in the unit-cell, according to nominal chemical composition. The missing lithium should probably be located mostly in the hollows surrounding the inversion centers (cf. the structure of α'-$LiZr_2(PO_4)_3$ (5)). A couple of minor broad negative peaks (with height of -0.13×10^{-12} cm) were actually present in that region of the last Fourier map, with fractional coordinates 0.42, 0.10, 0.01 and 0.17, 0.39, 0.10. However, in each case a too short distance (1.3 Å) with an O atom was observed, and it was not possible to refine their positions.

There is a slight overall unbalance of chemical composition, as total Fe and Ti are 1.075 and 0.925 atoms, respectively, instead of 1/1 as from the nominal stoichiometry (Table 3). We believe that this is related to difficulties in refining the parameters of site 1' (cf. the very large e.s.d.'s of Fe′, Ti′ atomic coordinates), which are due to the peculiarly unfavorable composition of the site with respect to neutron scattering lengths. As $b(Fe) = 0.954$ and $b(Ti) = -0.344 \times 10^{-12}$ cm, a composition of site 1′ with o.f.(Ti) ranging from 0.67 to 0.74 would give a *b* value for that site in the range 0.086 to -0.020×10^{-12} cm, i.e., very close to zero. This brings about a very small contribution to total scattering from site 1', causing in turn larger than usual uncertainties of the related structural parameters. Such difficulties add to the noteworthy complexity of the present crystal structure and to significant correlations between structural parameters due to pseudosymmetry, so as to explain the larger *R* values (Table 1) and differences between experimental and calculated profiles (Fig. 2) with respect to those obtained for $Li_2FeZr(PO_4)_3$ and for the polymorphs of $LiZr_2(PO_4)_3$ (5–7). This may also account for the failure to locate all lithium atoms in the unit-cell.

An insight into the crystal-chemical meaning of bond lengths r_i (Table 5) is favored by consideration of the corresponding bond valences s_i, according to $s_i = \exp[(r_i^0 - r_i)/0.37]$, where r_i^0 is an empirical parameter related to the pair of chemical species (21). The most striking feature which differentiates the two pseudo-symmetrical moieties of the asymmetric unit is the bonding of O5 and O5′. These oxygen atoms bridge pairs of adjacent slabs related by the *a* plane and pairs related by the inversion center, respectively; O5 is bonded to Li1, while O5' has no lithium bonding. The ensuing underbonding of O5' is only partially compensated by a much shorter P–O bond length (1.47(1) Å for P1′–O5′ against 1.62(1) Å for P1–O5), so that the corresponding sums of bond valences give 1.79 e (O5′) and 1.87 e (O5). Interestingly, both O atoms are still underbonded: this supports our belief (cf. above) that the missing lithium is preferentially accumulated in the interlayer region close to inversion centers and to O5′ atoms, but is also present in minor amounts in the other interlayer region where the *a* glide plane and the O5 atoms are present. The Li1 atom has a distorted tetrahedral coordination with quite regular Li–O bond distances, so that its bond valence balance closes up to 0.99 e.

The β Structure of $Li_2FeZr(PO_4)_3$

The content of two unit-cells of the crystal structure of $Li_2FeZr(PO_4)_3$ is shown in Fig. 4, so as to make the comparison with the superstructure of the Fe, Ti compound (Fig. 3) easier. All parallel slabs are related by *a* glide planes, and interlayer inversion centers are absent. Interatomic distances and O–Li–O angles are reported in Table 6. Li

TABLE 4
Atomic Fractional Coordinates and Isotropic Displacement Parameters of $Li_2FeZr(PO_4)_3$

	o.f.	*x*	*y*	*z*	*U* (10^{-2} Å^2)
Li	1	0.2814(18)	0.2214(17)	0.3233(13)	7.0(4)
Fe	0.5	0.7518(3)	0.4608(2)	0.6119(2)	0.86(5)
Zr	0.5	0.7518(3)	0.4608(2)	0.6119(2)	0.86(5)
P1	1	0.6057(4)	0.1061(4)	0.6473(3)	0.64(8)
P2	1	0.0418(6)	0.25	0.5	0.7(1)
O1	1	0.6581(4)	0.4318(3)	0.4675(3)	1.6(1)
O2	1	0.6611(4)	0.2646(3)	0.6797(2)	1.2(1)
O3	1	0.9438(3)	0.3579(4)	0.5682(3)	1.8(1)
O4	1	0.5688(4)	0.6030(3)	0.6586(3)	1.6(1)
O5	1	0.8234(4)	0.4873(3)	0.7755(3)	1.3(1)
O6	1	0.8551(3)	0.6588(3)	0.5771(3)	1.3(1)

Note. The e.s.d.s' are reported in parentheses.

TABLE 5
Interatomic Distances (Å) and O–Li–O′ Angles (°) in $Li_2FeTi(PO_4)_3$

Li1–O2	1.985(20)	O2–Li–O4	107.7(9)
O4	2.101(20)	O2–Li1–O5	80.3(8)
O5	1.993(21)	O2–Li1–O6	105.7(10)
O6	1.890(21)	O4–Li1–O5	121.7(10)
⟨Li1–O⟩	1.992	O4–Li1–O6	84.7(9)
		O5 –Li1–O6	150.5(11)
P1–O1	1.502(12)	P1′–O1′	1.524(11)
O2	1.499(11)	O2′	1.558(11)
O4	1.518(11)	O4′	1.515(11)
O5	1.621(11)	O5′	1.488(11)
⟨P1–O⟩	1.535	⟨P1′–O⟩	1.521
P2–O3	1.548(13)		
O6	1.556(13)		
O3′	1.524(13)		
O6′	1.473(11)		
⟨P2–O⟩	1.525		
Fe, Ti–O1′	1.928(11)	Fe′, Ti′–O1	1.833(25)
O2	2.149(11)	O2′	1.803(26)
O3	1.849(13)	O3′	2.052(29)
O4	2.038(12)	O4′	1.845(26)
O5	1.938(11)	O5′	2.163(27)
O6	1.918(13)	O6′	2.068(28)
⟨Fe, Ti–O⟩	1.970	⟨Fe′, Ti′–O⟩	1.961

Note. The e.s.d.'s are reported in parentheses.

appears here to be ordered on a single full-occupancy position, contributing to two atoms per formula-unit, unlike the case of β-$LiZr_2(PO_4)_3$ at 350°C (7), where Li was distributed over two sites (Li1 and Li2) with occupancies summing up to 0.5. However, the high Li displacement parameter (Table 4) could indicate a tendency toward a disordered arrangement similar to that of β-$LiZr_2(PO_4)_3$, possibly attained on heating. The coordination surroundings of Li here and Li1 in $Li_2FeTi(PO_4)_3$ are remarkably similar. By comparison, Li1 in β-$LiZr_2(PO_4)_3$ shows a more distorted coordination sphere, with much longer Li1–O2 and Li1–O4 bonds of 2.32 and 2.24 Å, respectively. An interesting result is that the Fe^{3+}/Zr^{4+} cations are fully disordered over a single available octahedral site, in spite of the larger difference of effective ionic radii (0.645 against 0.720 Å) with respect to the Fe^{3+}/Ti^{4+} pair (0.645 vs 0.605 Å), which shows a substantial ordering over two independent sites in the $Li_2FeTi(PO_4)_3$ structure. This point is related to the still unknown reasons making the latter compound prefer the α/β superstructure with respect to the β structure of the Fe, Zr material. A thorough investigation of the system $Li_{1+x}Fe_xM_{2-x}(PO_4)_3$ (M = Ti, Zr) with variable composition is under way to clarify the matter.

CONCLUSIONS

A new structural type has been determined and characterized by neutron diffraction in the family of NASICON-like

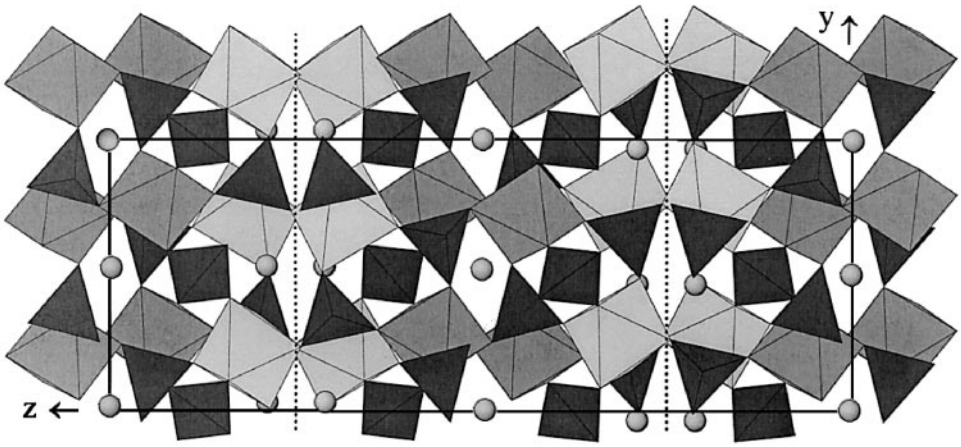

FIG. 3. Crystal structure of $Li_2FeTi(PO_4)_3$, projected onto the (100) plane. The PO_4 tetrahedra, (Fe, Ti)O_6 octahedra, and Li atoms (spheres) are emphasized. Dotted lines and isolated dots represent *a* glide planes and $\bar{1}$ inversion centeres, respectively.

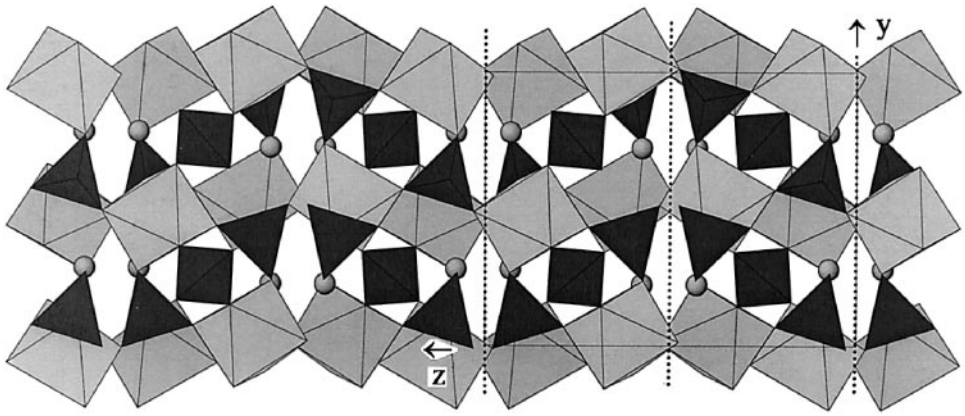

FIG. 4. Crystal structure of $Li_2FeZr(PO_4)_3$, projected onto the (100) plane. Dotted lines represent *a* glide planes.

lithium ion conductors, the α/β superstructure of $Li_2FeTi(PO_4)_3$, where α-type (inversion centers) and β-type (glide planes) (001) interslab regions alternate. The Ti^{4+} concentrates in the former, and Fe^{3+} in the latter region, respectively. Half of the Li^+ ions were located in the β-type interlayer, whereas the missing half probably lies in the α-type one. Bond valence considerations are consistent with the ordering scheme of octahedral cations and with the proposed lithium ion distribution in the interlayer regions. On the other hand, the corresponding Fe/Zr compound does not show this α/β superstructure but a β-type structure where, however, Li is fully ordered. This different behavior is probably related to the size ratio of trivalent and tetravalent octahedral cations, but it needs further investigation.

TABLE 6
Interatomic Distances (Å) and O–Li–O′ Angles (°) in $Li_2FeZr(PO_4)_3$

Li–O2	2.048(16)	O2–Li–O4	112.1(7)
O4	2.031(16)	O2–Li–O5	84.0(6)
O5	1.959(16)	O2–Li–O6	100.7(6)
O6	2.000(16)	O4–Li–O5	128.6(8)
⟨Li–O⟩	2.010	O4–Li–O6	85.2(6)
		O5–Li–O6	141.7(9)
P1–O1	1.512(4)	P2–O3	1.524(5) × 2
O2	1.526(5)	O6	1.528(5) × 2
O4	1.526(4)	⟨P2–O⟩	1.526
O5	1.536(5)		
⟨P1–O⟩	1.525		
Fe, Zr–O1	1.960(4)		
O2	2.069(4)		
O3	1.974(4)		
O4	2.103(4)		
O5	2.107(4)		
O6	2.004(4)		
⟨Fe, Zr–O⟩	2.036		

Note. The e.s.d.'s are reported in parentheses.

ACKNOWLEDGMENTS

Financial support from M.U.R.S.T. and C.N.R. (Italy) is gratefully acknowledged. We thank Norberto Morgante for his help with the synthesis and preliminary characterization of the phases studied in this work and Richard Ibberson for assistance with neutron diffraction measurements.

REFERENCES

1. C. Delmas, M. Ménétrier, L. Croguennec, S. Levasseur, J. P. Pérès, C. Pouillerie, G. Prado, L. Fournès, and F. Weill, *Int. J. Inorg. Mater.* **1,** 11 (1999).
2. A. D. Robertson, A. R. West, and A. G. Ritchie, *Solid State Ionics* **104,** 1 (1997).
3. J. Alamo, *Solid State Ionics* **63,** 547 (1993).
4. A. K. Padhi, V. Manivannan, and J. B. Goodenough, *J. Electrochem. Soc.* **145,** 1518(1998).
5. M. Catti, S. Stramare, and R. Ibberson, *Solid State Ionics* **123,** 173 (1999).
6. M. Catti and S. Stramare, *Solid State Ionics* **136–137,** 489 (2000).
7. M. Catti, N. Morgante, and R. M. Ibberson, *J. Solid State Chem.* **152,** 340 (2000).
8. A. B. Bykov, A. P. Chirkin, L. N. Demyanets, S. N. Doronin, E. A. Genkina, A. K. Ivanov-Shits, I. P. Kondratyuk, B. A. Maksimov, O. K. Mel'nikov, L. N. Muradyan, V. I. Simonov, and V. A. Timofeeva, *Solid State Ionics* **38,** 31 (1990).
9. T. Suzuki, K. Yoshida, K. Uematsu, T. Kodama, K. Toda, Z. Ye, and M. Sato, *Solid State Ionics* **104,** 27 (1997).
10. S. Wang and S. Hwu, *J. Solid State Chem.* **90,** 377 (1991).
11. S. Hamdoune, D. Tran Qui, and E. J. L. Schouler, *Solid State Ionics* **18/19,** 587(1986).
12. S. Hamdoune, M. Gondrand, and D. Tran Qui, *Mater. Res. Bull.* **21,** 237 (1986).
13. D. Tran Qui, S. Hamdoune, J. L. Soubeyroux, and E. Prince, *J. Solid State Chem.* **72,** 309 (1988).
14. M. Sugantha and U. V. Varadaraju, *Solid State Ionics* **95,** 201 (1997).
15. H. Aono, E. Sugimoto, Y. Sadaoka, N. Imanaka, and G. Adachi, *Solid State Ionics* **40/41,** 38 (1990).
16. C. M. Mari, R. Ruffo, and M. Catti, *J. Power Sources*, in press.

17. A. C. Larson and R. B. Von Dreele, "GSAS: Generalized Structure Analysis System Manual," Los Alamos National Laboratory Report LAUR: 86-748, 1994.
18. R. B. Von Dreele, J. D. Jorgensen, C. G. Windsor, *J. Appl. Crystallogr.* **15,** 581 (1982).
19. P. Thompson, D. E. Cox, and J. B. Hastings, *J. Appl. Crystallogr.* **20,** 79 (1987).
20. R. D. Shannon, *Acta Crystallogr. A* **32,** 751 (1976).
21. I. D. Brown and D. Altermatt, *Acta Crystallogr. B* (**41,** 244 (1985).